https://doi.org/10.5194/egusphere-2025-2981
Preprint. Discussion started: 27 June 2025

Radiative forcing and stratospheric ozone changes due to major forest fires and recent volcanic eruptions including Hunga Tonga

Christoph Brühl[1], Matthias Kohl[1], and Jos Lelieveld[1]

[1]Max Planck Institute for Chemistry, Mainz, Germany

Correspondence: christoph.bruehl@mpic.de

Abstract. Recent studies suggest that emissions from large forest fires affect stratospheric chemistry, dynamics, and climate, similar to major volcanic eruptions. Using the chemistry-climate model EMAC, we demonstrate that organic carbon emitted from forest fires, injected into the stratosphere through pyro-cumulonimbi, enhances heterogeneous chlorine activation due to increased solubility of HCl in particles containing organic acids and an augmented aerosol surface area. Following the 2019/2020 Australian megafires, the upward transport of the pollution plumes resulted in enhanced ozone depletion in the Southern Hemisphere lower stratosphere, as corroborated by satellite observations. It diminished column ozone in the following two years, accompanied by a dynamically induced reduction in 2020 due to the lofting of smoke-filled vortices, in total by up to 45 DU. The eruption of the submarine Hunga Tonga volcano in January 2022 caused a decline in total ozone across the entire Southern Hemisphere. The water vapour injection from the volcano altered only the vertical distribution of ozone loss. The sunlight-absorbing aerosol from the combined Australian and Canadian forest fire emissions in 2019/2020 induced the most significant perturbation in stratospheric optical depth since the major eruption of Pinatubo in 1991. It shifted the sign of instantaneous stratospheric aerosol forcing, derived at the top of the atmosphere, from -0.2 $\mathrm{W\,m^{-2}}$ to +0.3 $\mathrm{W\,m^{-2}}$ in January 2020. The global aerosol radiative forcing resulting from the Hunga Tonga eruption was -0.13 $\mathrm{W\,m^{-2}}$, primarily driven by changes in stratospheric sulfate aerosols. The positive radiative forcing from the injected water vapour was minimal.

1 Introduction

Since about 2017 it was observed that major forest fires which inject smoke particles via pyro-cumulonimbi directly into the midlatitude stratosphere can have a global impact on the radiation budget (Yu et al., 2021; Senf et al., 2023), stratospheric dynamics (Khaykin et al., 2020; Allen et al., 2020; Kablick et al., 2020; Santee et al., 2022), and chemistry of the stratosphere (Solomon et al., 2023; Ohneiser et al., 2022; Strahan et al., 2022; Salawitch and McBride, 2022; Ansmann et al., 2022). This holds for the Australian fires in December 2019 to January 2020 as well as Canadian fires in 2017 (Kloss et al., 2019; Doglioni et al., 2022) and 2019. There are also the Canadian fires in 2023. Vescovini et al. (2024) address the Californian fires in 2020 and the Siberian fires in 2019. The latter 3 events are not considered in our study.

Because of the absorbing aerosol the radiative impact of forest fire plumes differs from the one of major volcanic eruptions like for example Hunga Tonga in January 2022 (Taha et al., 2022). Radiative heating of the absorbing smoke particles causes self-lofting and in case of the Australian fires synoptic scale anticyclonic vortices lifting lower stratospheric and upper tropo-

https://doi.org/10.5194/egusphere-2025-2981
Preprint. Discussion started: 27 June 2025

spheric smoke containing airmasses with high N_2O and low ozone to the middle stratosphere (Allen et al., 2020; Kablick et al., 2020; Ma et al., 2024). Some of these vortices acting like a containment vessel transport the smoke particles to high latitudes. This and the about 10 km thick layer in the lower stratosphere perturbed by smoke cause a deeper Antarctic ozone hole due to heterogeneous chlorine activation (Cutts, 2023).

Hunga Tonga, the most explosive eruption since decades, has been analyzed in several studies. In January 2022 this submarine volcano injected huge amounts of water vapour directly into the middle stratosphere and even the lower mesosphere. Wang et al. (2023); Zhang et al. (2024) focus on enhanced ozone depletion due to enhanced aerosol surface area and water vapour using satellite observations and the WACCM-model. Santee et al. (2023, 2024) provide further references and observational data and some review of involved heterogeneous and gas phase chemistry. Zhu et al. (2023) analyse ozone depletion inside the plume, a process that we do not treat in our study.

With the chemistry climate model EMAC with extended heterogeneous chemistry on particles, introduced in section 2, we are able to reproduce most of the features observed by OSIRIS (Optical Spectrograph and InfraRed Imaging System), MLS (Microwave Limb Sounder), OMPS-LP (Ozone Mapping and Profiler Suite) and other satellite and balloon instruments and Lidar as shown in section 3. In this section we also discuss the radiative effects and stratospheric climate implications.

2 The chemistry climate model EMAC and used satellite data

2.1 EMAC and setup of the simulations

EMAC consists of the general circulation model ECHAM5 and the Modular Earth Submodel System MESSy V2.52 (Jöckel et al., 2010) including Atmospheric Chemistry. We use a setup in the spectral resolution T63 (1.9^o) with 90 layers up to 1 Pa (80 km) where the meteorology of the troposphere up to 100 hPa is nudged to the reanalysis ERA-5 (Hersbach et al., 2020) as recommended by Jöckel et al. (2006). Sea surface temperatures and sea ice cover are prescribed by ERA-5. The Quasi Biennial Oscillation (QBO) is internally generated but slightly nudged to observations compiled by the Free University of Berlin and Karlsruhe Institute of Technology (see https://www.atmohub.kit.edu/english/807.php, last accessed June 2025) to allow for a comparison with satellite data (Giorgetta et al., 2006).

The model contains interactive gas phase and heterogeneous chemistry and the aerosol microphysics module GMXE (Pringle et al., 2010) with 4 soluble and 3 insoluble modes with parameters as in Brühl et al. (2018) and EQSAM aerosol chemistry (Metzger and Lelieveld, 2007). Our module for heterogeneous chemistry on liquid stratospheric aerosol or polar stratospheric cloud (PSC) particles, MSBM, was modified as in Solomon et al. (2023), assuming that organic acids (e.g. hexanoic and acetic acids) in a particle strongly enhance the solubility of HCl in the particle compared to sulfuric acid or a mixture of sulfuric and nitric acid (Carslaw et al., 1995; Hanson et al., 1994; Huthwelker et al., 1995; Luo et al., 1995), accelerating the classical PCS reactions for chlorine activation also in midlatitudes. As in Solomon et al. (2023) the high solubility in hexanoic acid is applied if the mass ratio of organic carbon to sulfate exceeds 1. This leads to an HCl uptake and reactive chlorine release at much higher temperatures than for classical PSC or sulfate particles. The enhancement of surface area density (SAD) by organic aerosol leads also to faster conversion of NOx to HNO_3 via $N_2O_5 + H_2O \rightarrow 2\ HNO_3$.

https://doi.org/10.5194/egusphere-2025-2981
Preprint. Discussion started: 27 June 2025

The simulation is a continuation of the multidecadal transient simulation of Schallock et al. (2023) including several hundreds of explosive volcanic eruptions derived after March 2012 from OSIRIS extinction data. Kohl et al. (2024) contains a continuation of the volcanic emission inventory to 2023. For the powerful eruption of Hunga Tonga in January 2022 we assume that 400 kt SO_2 (Zhu et al., 2022) was injected near 25 km altitude based on the 3D plume seen by OSIRIS. A sensitivity study with 500 kt SO_2 and a slightly higher plume top height is also performed. The water vapour injection of 136 Mt by Hunga Tonga at 13-36 hPa is considered with the module TREXP (Jöckel et al., 2010; Kohl et al., 2024) assuming a Gaussian vertical distribution centered at 21.5 hPa and truncated at 2.4 σ with σ=1.25 km, and a slab covering 4 neighboring horizontal grid boxes, i.e. in total 48 boxes. Note that our estimate based on preliminary data is slightly less than the 146 Mt proposed by Millán et al. (2022). We also performed a sensitivity study with this amount and co-injected 500 kt SO_2 to study the chemical and radiative interactions.

Organic and black carbon (OC and BC) from the 3 major forest fires in 2017 to 2020 are injected in the Aitken mode at the top of the pyro-cumulonimbi into the lower stratosphere (1.5 km thick boxes) using TREXP with data from Peterson et al. (2018) for the British Columbia fire in August 2017, Osborne et al. (2022) for the Alberta fire in June 2019 and Peterson et al. (2021) for the Australian fire in December 2019 / January 2020. For the British Columbia fire we considered 4 3h events on August 12/13 emitting in total 300 kt OC and 19.5 kt BC in 4 slabs into the 132-175 hPa layer at slightly different locations and times near 51^{o}N/122^{o}W. The smoke of the Alberta fire is injected on June 17 in the same altitude range into 4 neighboring slabs near 60.5^{o}N/116^{o}W with in total 108 kt OC and 7 kt BC. The Australian fire was modeled as a 63 h lasting event starting on December 29 injecting 600 kt OC and 39 kt BC into the layer between 92 and 121 hPa covering 4 horizontal gridboxes around 37^{o}S/149^{o}E, followed by a 6 h event on January 4 injecting 216 kt OC and 13.8 kt BC into the same slabs. Organic carbon is assumed to be in the soluble and black carbon in the insoluble mode. The absorbing smoke particles experience lofting by radiative heating reaching about 28 km in case of the Australian fire.

2.2 OSIRIS

OSIRIS is a limb scatter observing instrument, which was launched on board the Odin satellite on 20 February 2001 and is still operating today. OSIRIS provides coverage from 82^{o}S to 82^{o}N over the course of the year. To obtain the vertical profiles of aerosol extinction at altitudes from 10 to 35 km, the aerosol scattering properties are calculated with a refractive index of $1.427+i7.167\times10^{-8}$ using Mie theory at 750 nm wavelength and a sulfate concentration of 75% H_2SO_4 and 25% H_2O (Rieger et al., 2019). Extinction is retrieved where the tangent point is illuminated, which is primarily in the summer hemisphere, using version 7.3. The grid resolution is 1 km altitude, 5^o latitude, and 30^o longitude with 5 day averaged time intervals. Observed zonal average stratospheric aerosol optical depth (SAOD) for 3 latitude ranges and 5 years is shown by the green curves in Fig. 1.

2.3 OMPS-LP

The OMPS-LP instrument on the Suomi National Polar Orbiting satellite, which was launched in 2011, measures vertical images of the spectral radiance of the atmospheric limb. These scattered-sunlight spectra, in the range 290–1,000 nm, are

https://doi.org/10.5194/egusphere-2025-2981
Preprint. Discussion started: 27 June 2025

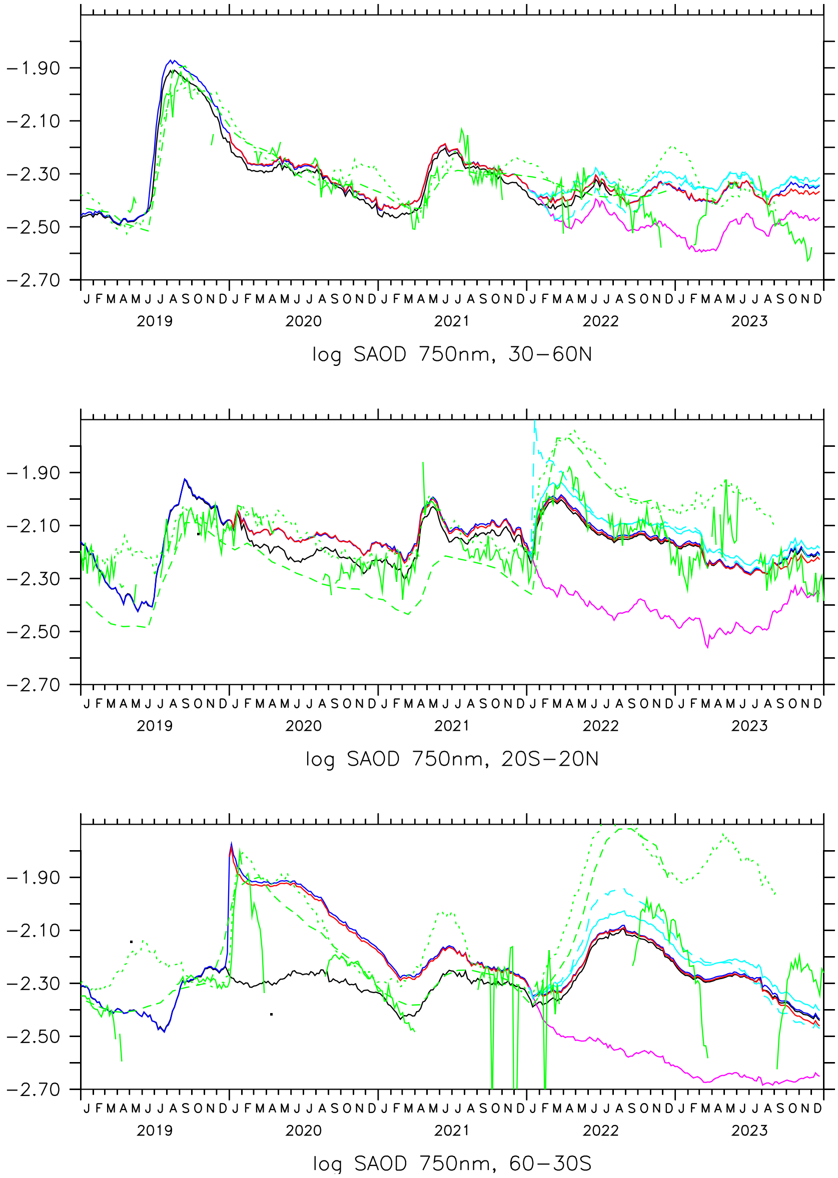

Figure 1. Stratospheric aerosol optical depth in tropical latitudes (middle), northern (upper) and southern midlatitudes (lower), zonal 5 day averages. Black: EMAC without fires, blue: EMAC with 3 major fires (w/o heterogeneous chemistry on organic aerosol), red: EMAC with heterogeneous chemistry on smoke particles, light blue: same with 500 kt of SO_2 from Hunga Tonga, light blue dashed: same but SO_2 co-injected with H_2O, purple: EMAC without Hunga Tonga, green: observed by OSIRIS, green dashed: GloSSAC, green dotted: observed by OMPS-LP.

used in combination with a radiative transfer forward model to retrieve vertical profiles of ozone number density and aerosol extinction coefficient. Measurements are made along the daylight portion of the satellite orbital track. Aerosol extinction

https://doi.org/10.5194/egusphere-2025-2981
Preprint. Discussion started: 27 June 2025

is retrieved at a single wavelength channel of 746 nm, derived using a two-dimensional, or tomographic, inversion (Rieger et al., 2021; Bourassa et al., 2023). The vertical and horizontal resolutions of the retrieval are approximately 1.5 and 250 km, respectively, and profiles generally extend from the tropopause through the upper stratosphere. Here we use L2-version 1.3, the grid resolution is like for the OSIRIS data set. Zonal average observations of SAOD are shown by the green dotted curves in Fig. 1.

2.4 AURA-MLS

MLS onboard NASA's Aura satellite provides measurements of 15 trace gases, among them H_2O, HCl, HNO_3 and O_3. Here we use version 5 following Santee et al. (2023). MLS measures thermal emission from the Earth's limb, covering spectral regions near 118, 190, 240, and 640 GHz. We use zonal average daily gridded L3 data on pressure levels with a resolution of 4^o in latitude and about 2.4 km in altitude (Livesey et al., 2022).

3 Results for 2019-2023

We performed a transient simulation without forest fires, simulations with the radiative and dynamical effects of the forest fires mentioned in section 2, with and without the eruption of Hunga Tonga, and simulations with heterogeneous chemistry on organic aerosol for the standard Hunga Tonga case and the 2 sensitivity studies with more SO_2 addressed above.

3.1 Optical depth, radiative forcing and heating

Simulated and observed stratospheric aerosol optical depth (SAOD) for tropics and southern and northern midlatitudes is presented in Fig. 1. Considering the organic aerosol from major forest fires is essential for agreement with the observations by OSIRIS. In southern midlatitudes the Australian forest fire enhances SAOD in January 2020 in observation and simulation by about 0.011 in zonal mean, and 2 years later the perturbation is still 0.0005 as can be seen by the green, black and red curves, consistent also with lidar observations by Ohneiser et al. (2022). In northern midlatitudes, SAOD is dominated by the eruption of Raikoke in 2019 while Canadian fires cause a slight enhancement. The eruption of Hunga Tonga in January 2022 dominates SAOD in the next years. In the tropics the eruptions of Ulawun in June and August 2019 and of St. Vincent in April 2021 have also a large impact on SAOD while the effect of Australian fires with up to 0.0013 is relatively small. Note that the very low OSIRIS values near the data gaps in midlatitudes are artifacts due to sparse coverage, values at very large solar zenith angles and often missing observations of the lowermost stratosphere and should be ignored. Also, this feature does not happen in OMPS-LP observations (Rieger et al., 2021; Bourassa et al., 2023) and GloSSAC (Kovilakam et al., 2023). However, OMPS-LP observations sometimes appear to be high-biased compared to other instruments. During northern summer 2020 OSIRIS data were so sparse that OMPS-LP had to be used to estimate SO_2 injections of some volcanic events and it looks like that the used factors "f" (Schallock et al., 2023) for these were too large, leading to an overestimate of the sulfate contribution to extinction still visible to the end of 2020 in the southern hemisphere. In April 2023 there appears to be a southern midlatitude volcanic event missing in our inventory or the Hunga Tonga SO_2 injection is underestimated. Also in April 2023 some source

https://doi.org/10.5194/egusphere-2025-2981
Preprint. Discussion started: 27 June 2025

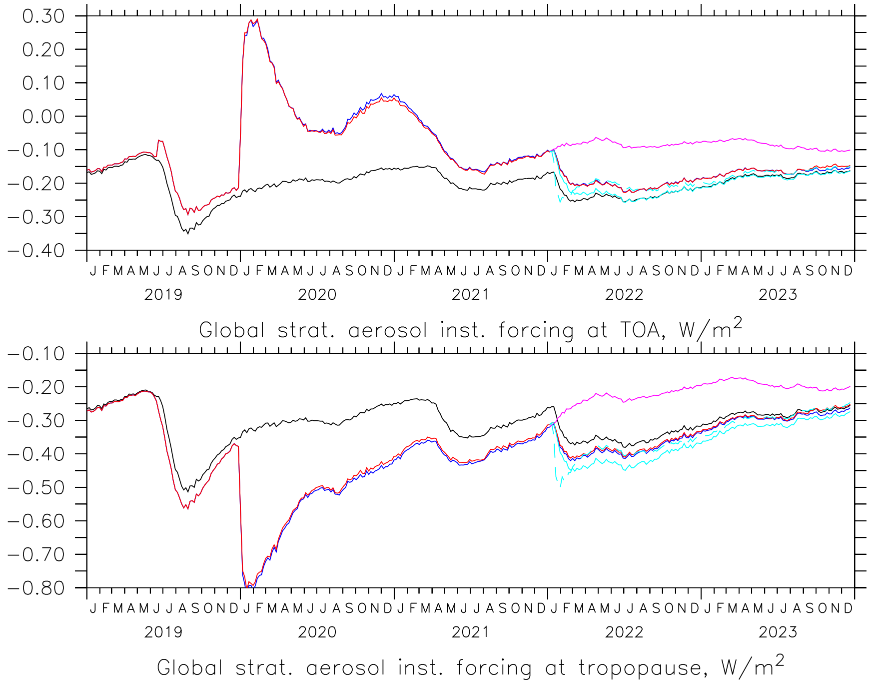

Global strat. aerosol inst. forcing at TOA, W/m^2

Global strat. aerosol inst. forcing at tropopause, W/m^2

Figure 2. Calculated instantaneous radiative forcing by aerosol at the Top of the Atmosphere (TOA, upper) and tropopause altitude (lower). Black: EMAC without fires, blue: EMAC with fires, purple: no Hunga Tonga, red: EMAC with heterogeneous chemistry on smoke particles, lightblue: as red but 500kt SO_2, lightblue dashed: same but SO_2 co-injected with H_2O.

of aerosol is missing in the tropics. The sensitivity study with enhanced SO_2 injection by Hunga Tonga improves the agreement with OSIRIS observations in late 2022, but still underestimates SH midlatitude SAOD in 2023. Ignoring Hunga Tunga reduces SAOD by up to 0.0060 to 0.0075. In the sensitivity study where SO_2 is co-injected with H_2O the strongly enhanced OH production leads to a very quick sulfur aerosol formation causing the too early peak of SAOD in the tropics. Radiative heating of this aerosol causes a lofting of the plume and a faster spread to midlatitudes leading to a better agreement of SAOD with GloSSAC there.

The global instantaneous stratospheric aerosol forcing calculated online by multiple radiation calls at the top of the atmosphere (TOA) and in the altitude of the midlatitude tropopause is shown in Fig. 2. The Australian fire emissions change the TOA forcing by up to 0.5 $\mathrm{W\,m^{-2}}$ in January 2020 with the perturbation modulated by insolation lasting more than 3 years with values of 0.07 $\mathrm{W\,m^{-2}}$ in January 2022 and 0.02 $\mathrm{W\,m^{-2}}$ in January 2023. The small signal after July 2019 is related to Canadian fires. The sign change of the forcing perturbation by smoke with altitude is due to its light absorbing properties. The computed global aerosol radiative forcing caused by the Hunga Tonga eruption in 2022 was about -0.12 $\mathrm{W\,m^{-2}}$, decreasing to -0.06 $\mathrm{W\,m^{-2}}$ by December 2023, dominated by the change in stratospheric sulfate aerosols. In the sensitivity simulation

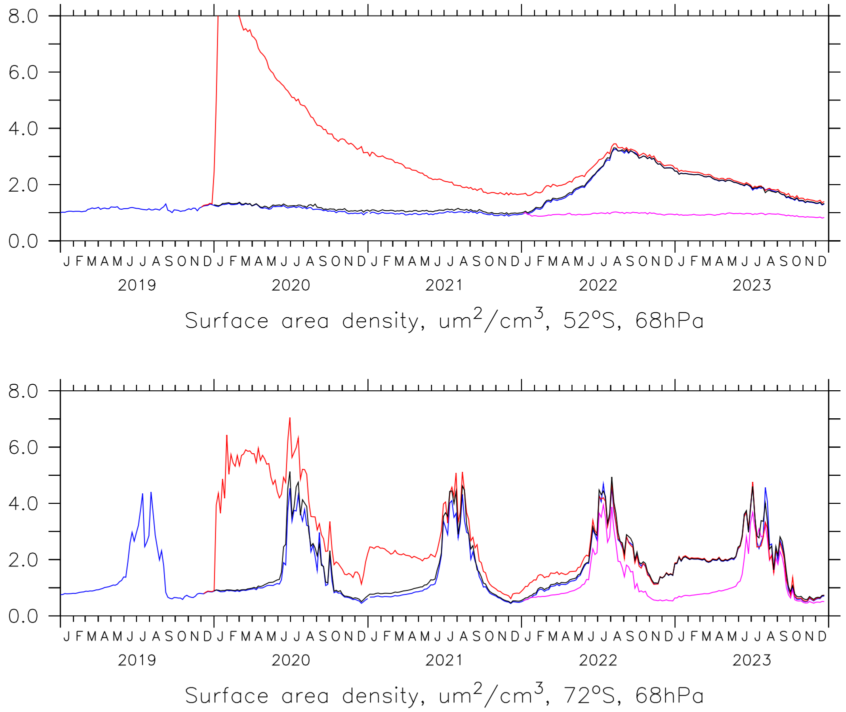

Figure 3. Calculated surface area density [μm^2/cm^3] in the lower stratosphere in southern middle and high latitudes. Black: sulfate and PSCs only; Blue: sulfate and PSCs only with dynamical effect of smoke; Purple: without Hunga Tonga; Red: Including smoke particles.

with more Hunga Tonga SO_2 these numbers change to -0.14 W m^{-2} and -0.07 W m^{-2}. In the experiment with co-injection the effect of Hunga Tonga is larger in the first 2 months and smaller later, approaching the 400 kt SO_2 scenario.

Solar and infrared radiative heating rates by smoke and volcanic aerosol in tropics and midlatitudes in Figs. A6 and A7 are largest in the middle stratosphere with up to 0.11 K/d at 28 km in the tropics and 0.36 K/d at 20 km in midlatitudes in zonal average. The heating by smoke from the Australian fires leads to a zonal average temperature increase of up to about 3 K over several months in large parts of the SH lower stratosphere. This feature is similar to that reported by Yu et al. (2021). The warmer tropopause region causes also an increase in stratospheric water vapour (Fig. A1). Hunga Tonga causes a heating rate by up to 0.025 K/d at 25 km in the tropics and 0.011 K/d in southern midlatitudes. The heating by up to 0.032 K/d in the tropics at 18 km is related to the eruptions of Ulawun and St. Vincent.

3.2 Perturbation of dynamics by smoke

In case of the Australian fires the strong radiative heating in the absorbing aerosol containing plumes causes their lofting and the formation of anticyclonic vortices. The vortices generated by EMAC are similar in size as the observed ones discussed in Kablick et al. (2020) but the location differs and the lofting is somewhat faster. EMAC reproduces the reduced ozone and

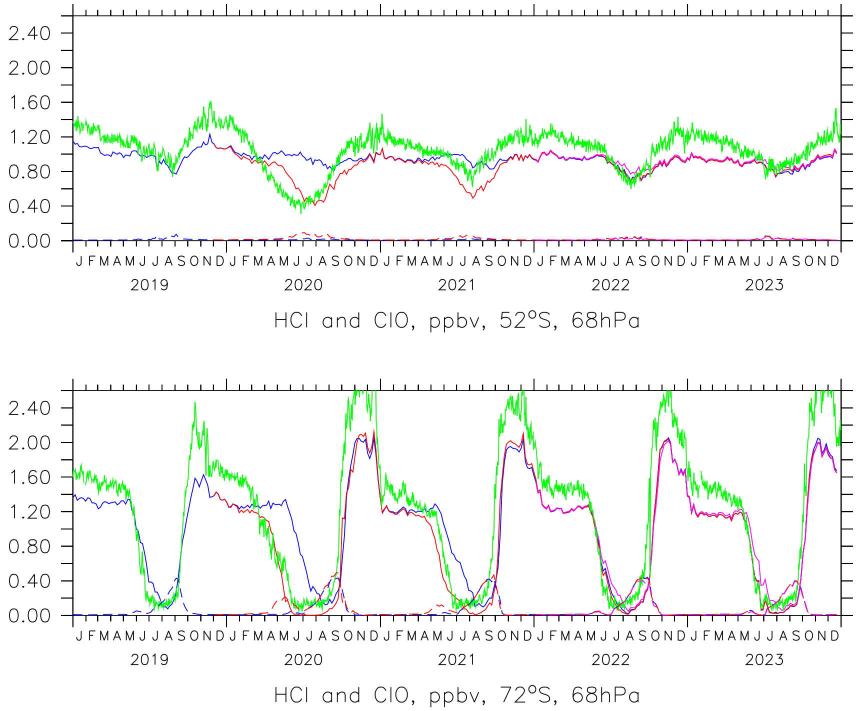

Figure 4. Simulated and observed HCl at 68 hPa at 52^{o}S (upper) and 72^{o}S (lower). Blue: EMAC with Hunga Tonga including water and dynamical effects of fires, Purple: EMAC without Hunga Tonga, Red: EMAC with Hunga Tonga and enhanced heterogeneous chlorine activation on organic particles. Green: MLS observations. Black curve for EMAC without fires not shown because very close to the blue one. Dashed curves for calculated ClO (MLS not shown). 5 day averages for EMAC, daily averages for MLS.

enhanced N_2O in the smoke filled vortices due to vertical displacement. An example for January 2020 and southern midlatitudes is shown in Figs. A8 and A9. These perturbations are visible for about 2 months. In the used setup of the model the vortices rise only to about 28 km, the maximum altitude where heating by aerosol is considered in the radiation scheme. Because of this limitation the perturbations found by Ma et al. (2024) above this altitude could not be studied.

3.3 Aerosol properties and ozone chemistry

Calculated number densities N and median wet radii r_{median} in the accumulation mode in tropics and SH midlatitudes are presented in Figs. A4 and A5. N increases by up to about 50% for the Australian fire and by up to 100% for Hunga Tonga at 52^{o}S and 68 hPa, for r_{median} the increase there is about 0.03 μm for both perturbations.

The simulated particle surface area density (SAD) for use with heterogeneous chemistry is shown in Fig. 3. The organic particles injected into the stratosphere by the Australian fires cause a large enhancement of SAD by up to about a factor of 10 in the whole Southern hemisphere. In the calculation we assume here the molecular mass of acetic acid. Hunga Tonga is

https://doi.org/10.5194/egusphere-2025-2981
Preprint. Discussion started: 27 June 2025

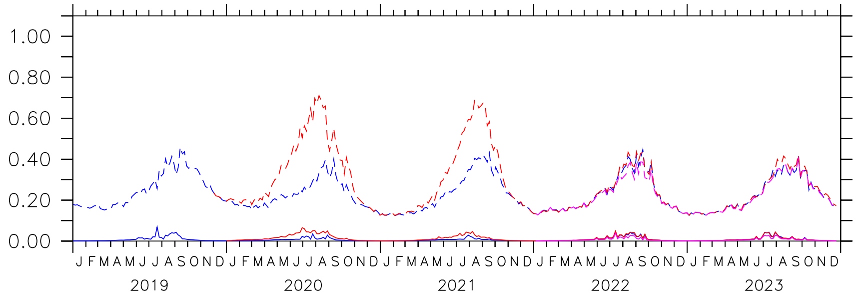

HOCl and ClNO$_3$, ppbv, 52°S, 68hPa

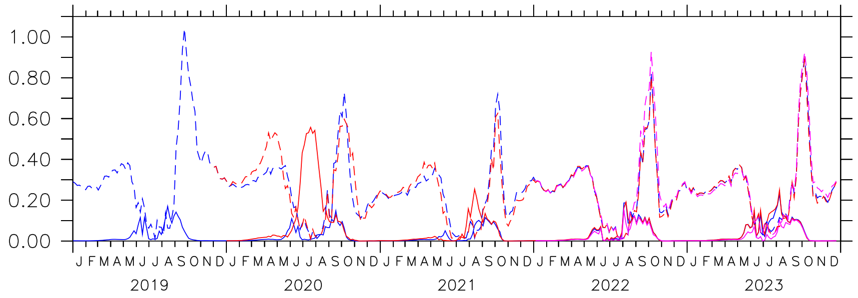

HOCl and ClNO$_3$, ppbv, 72°S, 68hPa

Figure 5. Simulated HOCl at 68 hPa at 52^{o}S (upper) and 72^{o}S (lower). Blue: EMAC with Hunga Tonga including water and dynamical effects of fires, Purple: EMAC without Hunga Tonga, Red: EMAC with Hunga Tonga and enhanced heterogeneous chlorine activation on organic particles. Black curve for EMAC without fires not shown because very close to the blue one. Dashed curves show calculated ClONO$_2$.

responsible for about a doubling to tripling of SAD outside the regions with polar stratospheric clouds (PSC, causing the winter peaks) at 68 hPa.

Simulated and observed HCl and simulated ClO for mid and high southern latitudes are depicted in Fig. 4, simulated HOCl and ClONO$_2$ in Fig. 5. It is clearly seen that heterogeneous chlorine activation on organic particles has to be included to reproduce the HCl observations by MLS with a fast decrease in Austral fall and early winter of 2020 and 2021 (red and green curves) accompanied by an increase in ClO. In the presence of organic aerosol in these winters ClONO$_2$ is strongly enhanced in midlatitudes and HOCl in high latitudes. Heterogeneous chlorine activation on Hunga Tonga aerosol is important in Austral winters of 2022 and 2023 (blue/red curves against purple ones). For the nitrogen species mostly the effect of the SAD increase due to smoke and volcano matters, causing an increase in HNO$_3$ (Fig. 6) and a decrease in NO$_2$ (Fig. A2). For HNO$_3$ the EMAC simulations match almost perfectly with the MLS observations if the heterogeneous chemistry on smoke aerosol is included (Fig. 6). The reduction of NOx by heterogeneous reactions on organic and sulfate aerosol leads to an increase in the hydroxy radical due to NO + HO$_2$ → NO$_2$ + OH (Fig. A3). This effect and the Hunga Tonga water vapour injections and the subsequent increase in stratospheric water vapour (Fig. A1) cause an enhancement in HO$_2$ by almost 20% in Austral summers of 2022/2023 and 2023/2024.

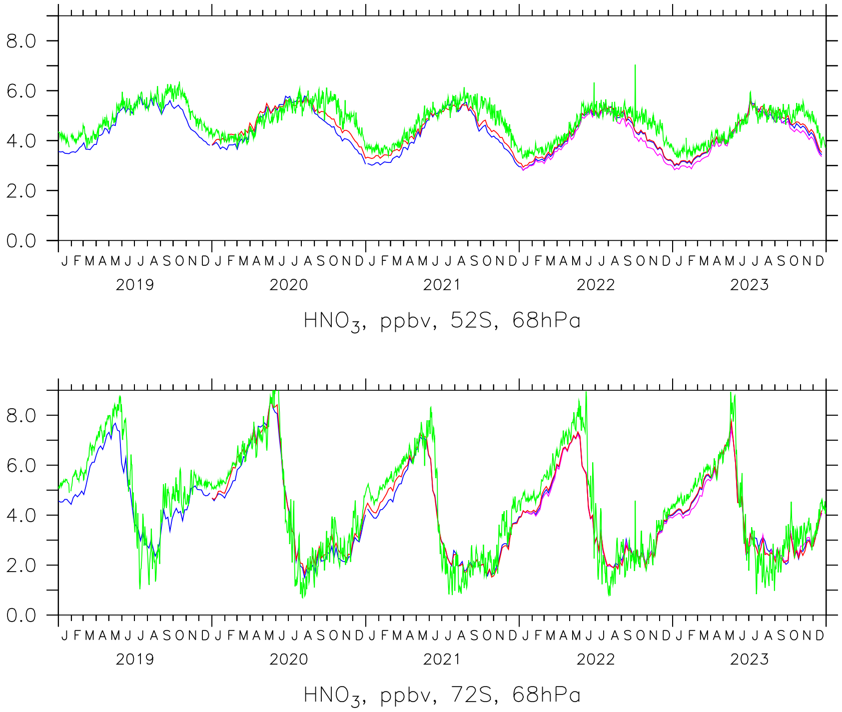

Figure 6. As Fig. 4 but for HNO_3.

Simulated and observed ozone is shown in Fig. 7. Here the combined effect of perturbation of dynamics and chemistry by smoke causes a zonal average decrease of almost 10% in the midlatitude lower stratosphere and almost complete loss at the edge of the ozone hole in winter 2020 in agreement with MLS (black, red and green curves). The effect of Hunga Tonga is mostly visible at the vortex edge (purple and blue curves).

Heterogeneous chlorine activation causes decreases in zonally averaged total ozone of more than 30 DU in the first 2 years after the Australian fires (Fig. 8a), Changes in dynamics due to heating by smoke cause a total ozone decrease by up to about 20 DU (Fig. 8c), combined effects add up to a loss of up to 45 DU. At 50^{o}S the typical decrease in Austral winter still exceeds 10 DU. The loss due to the eruption of Hunga Tonga is up to about 15 DU in 2022 and 2023 (Fig. 8b).

4 Conclusions

The Australian forest fires in 2019/2020 caused the largest perturbation in stratospheric optical depth (for example, in OSIRIS and OMPS-LP data) and instantaneous radiative forcing since the eruption of Pinatubo by up to 0.5 $\mathrm{W\,m^{-2}}$ at the top of the atmosphere and -0.4 $\mathrm{W\,m^{-2}}$ at the tropopause. In January 2022, the remaining effect at TOA was about 0.05 $\mathrm{W\,m^{-2}}$, still counteracting the negative forcing by volcanoes, which was in case of Hunga Tonga up to -0.14 $\mathrm{W\,m^{-2}}$. These fires

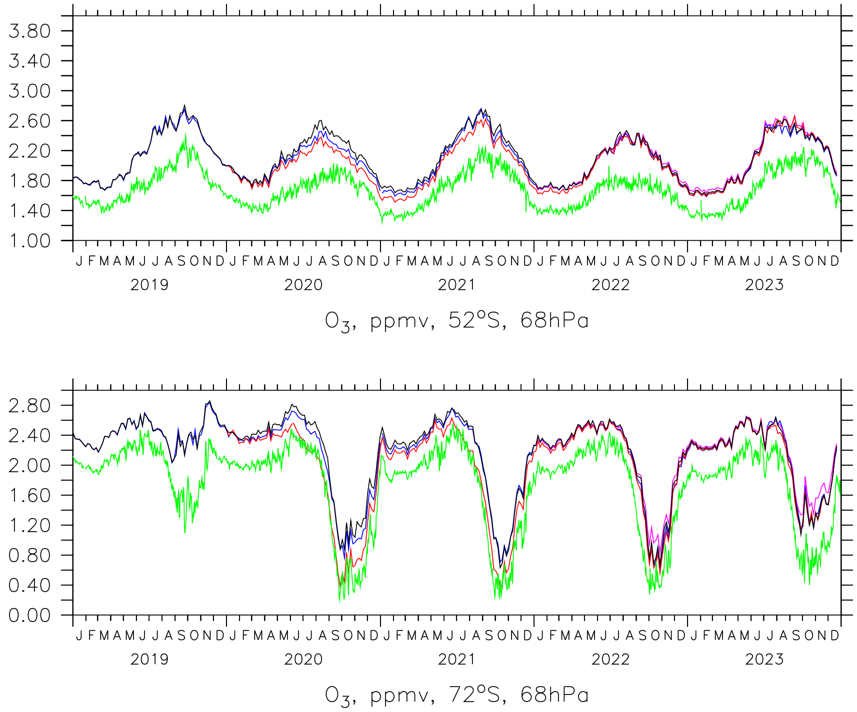

Figure 7. As Fig.4 but for ozone, black without fires.

caused a zonal average heating of the lower stratosphere of the Southern Hemisphere by up to about 3 K for several months. The absorbing aerosol from the Boreal fires in 2017 and 2019 reduced the volcanic forcing at TOA but enhanced it at the tropopause. It is needed to explain the observed AOD.

To obtain agreement with the chlorine activation in polar regions observed by MLS it is essential to include the enhanced solubility of HCl in particles containing organic acids from major forest fires. The Australian fire emissions led to enhanced ozone depletion in fall, winter and spring in high and mid latitudes reducing minimum total ozone in 2020 and 2021 by up to 28 DU around 70^{o}S, accompanied by a reduction in August 2020 from the lofting smoke filled vortices and other perturbations in dynamics by up to 24 DU (total up to about 45 DU).

The total ozone loss due to the eruption of Hunga Tonga was up to about 15 DU in 2022 and 2023. Hunga Tonga water vapour had only a small effect on ozone and radiative forcing. EMAC reproduces the water vapour increase seen by MLS but has a low bias of almost 1 ppmv (outside of the Antarctic vortex, Fig. A1). Co-injection of SO_2 and H_2O leads to features not observed since it almost prevents the descent of the H_2O plume by radiative cooling in the early phase due to heating of the sulfur aerosol which is formed too rapidly, related to strongly enhanced OH, which leads to a too late arrival of the additional water vapour in the lower stratosphere at mid and high southern latitudes. However, some overlap of the H_2O and SO_2 plumes needs to be assumed to explain the observed fast SO_2 conversion (Santee et al., 2023). For ozone the water vapour increase

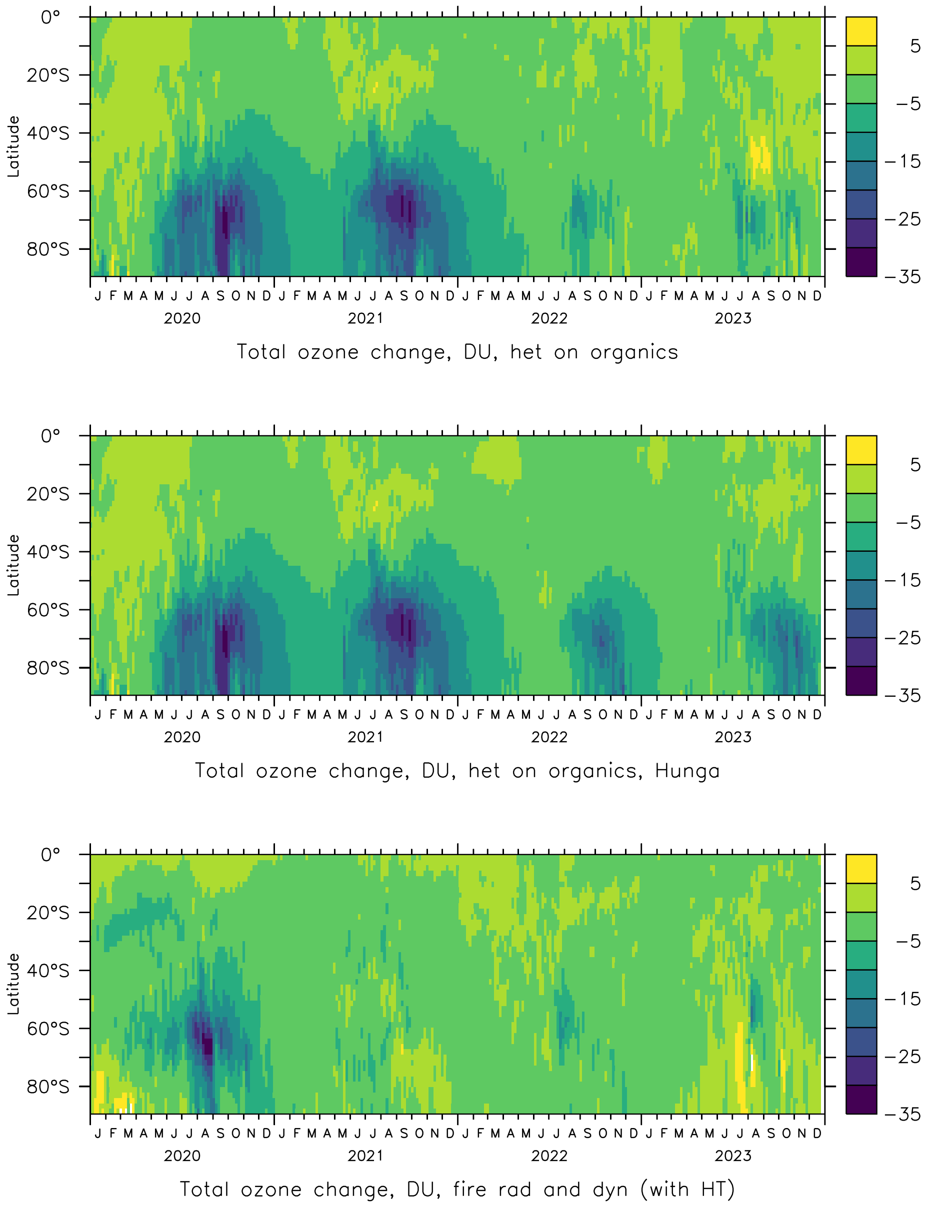

Figure 8. Calculated total ozone change from heterogeneous chlorine activation on organics from fires (upper, a) and additionally the eruption of Hunga Tonga (middle, b). The lower panel (c) shows the radiative/dynamical effects of fires (in 2023 mostly noise).

causes a change in the vertical distribution with almost no effect on total ozone, while the positive radiative forcing is not significant in the model.

We demonstrated that EMAC (in this version) is a useful tool for simulating the implications of major forest fires and volcanic eruptions on climate and stratospheric ozone, including the delay in the recovery of the Antarctic ozone hole.

Code and data availability. The Modular Earth Submodel System (MESSy) is continuously developed and used by a consortium of institutions. The use of MESSy and access to the source code is licensed to all affiliates of institutions which are members of the MESSy Consortium. Institutions can become a member of the MESSy Consortium by signing the MESSy Memorandum of Understanding. More information can be found on the MESSy Consortium website (http://www.messy-interface.org, last accessed June 2025). The code, namelists, input data files and model output of EMAC used here are stored at DKRZ, Hamburg, Germany.

The complete OSIRIS L2 data set can be downloaded from https://arg.usask.ca/docs/osiris_v7/, the OMPS-LP L2 aerosol extinction data from https://doi.org/10.5281/zenodo.7293121 (gridded data for both instruments can be requested from the authors). AURA-MLS L3 data (V5, gridded on pressure levels, daily) are available from Goddard Earth Sciences Data and Information Services Center (GES DISC, https://data.gesdisc.earthdata.nasa.gov/data/Aura_MLS_Level3).

Author contributions. CB modified the code, performed the simulations and wrote most of the paper, MK contributed to the setup of the volcano and wild fire emissions and the text, JL worked on the text.

Competing interests. The authors declare that they have no conflicts of interest.

Acknowledgements. We thank Landon Rieger, now at Canadian Centre for Climate Modelling and Analysis (CCCma), Environment and Climate Change Canada (ECCC), Victoria, BC, Canada, for providing OSIRIS and OMPS-LP data in the early phase of the paper, Adam Bourassa, University of Saskatchewan, Saskatoon, Canada, for advices to the OSIRIS and OMPS-LP data, and Michelle Santee, Jet Propulsion Laboratory, California Institute of Technology, Pasadena, CA, USA for help with MLS data and useful suggestions for the introduction. AGAGE observations are used as lower boundary condition for long lived gases in EMAC. The computations were performed on the Levante supercomputer at DKRZ Hamburg, Germany, with support by Max Planck Society.

References

Allen, D. R., Fromm, M. D., Kablick III, G. P., and Nedoluha, G. E.: Smoke with Induced Rotation and Lofting (SWIRL) in the Stratosphere, J. Atmos. Sci., 77, 4297–4316, https://doi.org/10.1175/JAS-D-20-0131.1, 2020.

Ansmann, A., Ohneiser, K., Chudnovsky, A., Knopf, D. A., Eloranta, E. W., Villanueva, D., Seifert, P., Radenz, M., Barja, B., Zamorano, F., Jimenez, C. Engelmann, R., Baars, H., Griesche, H., Hofer, J., Althausen, D., and Wandinger, U.: Ozone depletion in the Arctic and Antarctic stratosphere induced by wildfire smoke, Atmos. Chem. Phys., 22, 11 701–11 726, https://doi.org/10.5194/acp-22-11701-2022, 2022.

Bourassa, A. E., Zawada, D. J.and Rieger, L. A., Warnock, T. W., Toohey, M., and Degenstein, D. A.: Tomographic retrievals of Hunga Tonga-Hunga Ha'apai volcanic aerosol, Geophys. Res. Lett., 50, https://doi.org/10.1029/2022GL101978, 2023.

Brühl, C., Schallock, J., Klingmüller, K., Robert, C., Bingen, C., Clarisse, L., Heckel, A., North, P., and Rieger, L.: Stratospheric aerosol radiative forcing simulated by the chemistry climate model EMAC using Aerosol CCI satellite data, Atmos. Chem. Phys., 18, 12 845–12 857, https://doi.org/10.5194/acp-18-12845-2018, 2018.

Carslaw, K. S., Clegg, S. L., and Brimblecombe, P.: A thermodynamic model of the system HC1-HNO_3-H_2SO_4-H_2O, including solubilities of HBr, from <200 to 328 K, J. Phys. Chem., 99, 11 557–11 574, https://doi.org/10.1021/j10029a039, 1995.

Cutts, E.: Wildfire smoke destroys ozone, EOS, 104, https://doi.org/10.1029/2023EO230148., 2023.

Doglioni, G., Aquila, V., Das, S., Colarco, P. R., and Zardi1, D.: Dynamical perturbation of the stratosphere by a pyrocumulonimbus injection of carbonaceous aerosols, Atmos. Chem. Phys., 22, 11 049–11 064, https://doi.org/10.5194/acp-22-11049-2022, 2022.

Giorgetta, M. A., Manzini, E., Roeckner, E., Esch, M., and Bengtsson, L.: Climatology and forcing of the quasi-biennial oscillation in the MAECHAM5 model, J. Climate, 19, 3882–3901, https://doi.org/10.1175/JCLI3830.1, 2006.

Hanson, D. R., Ravishankara, A. R., and Solomon, S.: Heterogeneous reactions in sulfuric acid aerosols: A framework for model calculations, J. Geophys. Res. -Atmos., 99, 3615–3629, https://doi.org/10.1029/93JD02932, 1994.

Hersbach, H., Bell, B., Berrisford, P., Hirahara, S., Horányi, A., Muñoz-Sabater, J., Nicolas, J., Peubey, C., Radu, R., Schepers, D., Simmons, A., Soci, C., Abdalla, S., Abellan, X., Balsamo, G., Bechtold, P., Biavati, G., Bidlot, J., Bonavita, M., De Chiara, G., Dahlgren, P., Dee, D., Diamantakis, M., Dragani, R., Flemming, J., Forbes, R., Fuentes, M., Geer, A., Haimberger, L., Healy, S., Hogan, R. J., Hólm, E., Janisková, M., Keeley, S., Laloyaux, P., Lopez, P., Lupu, C., Radnoti, G., de Rosnay, P., Rozum, I., Vamborg, F., Villaume, S., and Thépaut, J.-N.: The ERA5 global reanalysis, Quarterly Journal of the Royal Meteorological Society, 146, 1999–2049, https://doi.org/https://doi.org/10.1002/qj.3803, 2020.

Huthwelker, T., Peter, T., Luo, B. P., Clegg, S. L., Carslaw, K. S., and Brimblecombe, P.: Solubility of HOC1 in water and aqueous H_2SO_4 to stratospheric temperatures, J. Atmos. Chem., 21, 81–95, https://doi.org/10.1007/BF00712439, 1995.

Jöckel, P., Tost, H., Pozzer, A., Brühl, C., Buchholz, J., Ganzeveld, L., Hoor, P., Kerkweg, A., Lawrence, M. G., Sander, R., Steil, B., Stiller, G., Tanarhte, M., Taraborrelli, D., van Aardenne, J., and Lelieveld, J.: The atmospheric chemistry general circulation model ECHAM5/MESSy1: consistent simulation of ozone from the surface to the mesosphere, Atmos. Chem. Phys., 6, 5067–5104, https://doi.org/10.5194/acp-6-5067-2006, 2006.

Jöckel, P., Kerkweg, A., Pozzer, A., Sander, R., Tost, H., Riede, H., Baumgaertner, A., Gromov, S., and Kern, B.: Development cycle 2 of the Modular Earth Submodel System (MESSy2), Geosci. Model Dev., 3, 717–752, https://doi.org/10.5194/gmd-3-717-2010, 2010.

Kablick, G. P., Allen, D. R., Fromm, M. D., and Nedoluha, G. E.: Australian PyroCb smoke generates synoptic-scale stratospheric anticyclones, Geophys. Rese. Lett., 47, e2020GL088 101, https://doi.org/10.1029/2020GL088101, 2020.

https://doi.org/10.5194/egusphere-2025-2981
Preprint. Discussion started: 27 June 2025

Khaykin, S., Legras, B., Bucci, S., Sellitto, P., Isaksen, L., Tencé, F., Bekki, S., Bourassa, A., Rieger, L., Zawada, D., Jumelet, J., and Godin-Beekmann, S.: The 2019/20 Australian wildfires generated a persistent smoke-charged vortex rising up to 35 km altitude, Commun. Earth Environ., 1, 1–12, https://doi.org/10.1038/s43247-020-00022-5, 2020.

Kloss, C., Berthet, G., Sellitto, P., Ploeger, F., Bucci, S., Khaykin, S., Jégou, F., Taha, G., Thomason, L. W., Barret, B., Le Flochmoen, E., Von Hobe, M., Bossolasco, A., Bègue, N., and Legras, B.: Transport of the 2017 canadian wildfire plume to the tropics via the asian monsoon circulation, Atmos. Chem. Phys., 19, 13 547–13 567, https://doi.org/10.5194/acp-19-13547-2019, 2019.

Kohl, M., Brühl, C., Schallock, J., Tost, H., Jöckel, P., Jost, A., Beirle, S., Höpfner, M., and Pozzer, A.: New submodel for emissions from Explosive Volcanic ERuptions (EVER v1.1) within the Modular Earth Submodel System (MESSy, version 2.55.1), EGUsphere, https://doi.org/10.5194/egusphere-2024-2200, 2024.

Kovilakam, M., Thomason, L., and Knepp, T.: SAGE III/ISS aerosol/cloud categorization and its impact on GloSSAC, Atmos. Meas. Tech., 16, 2709–2731, https://doi.org/10.5194/amt-16-2709-2023, 2023.

Livesey, N. J., Read, W. G., Wagner, P. A., Froidevaux, L., Santee, M. L., Schwartz, M. J., Lambert, A., Millán Valle, L. F., Pumphrey, H. C., Manney, G. L., Fuller, R. A., Jarnot, R. F., Knosp, B. W., and Lay, R. R.: Version 5.0x Level 2 and 3 Data Quality and Description Document (No. JPL D-105336 Rev. B), Tech. rep., Jet Propulsion Laboratory, http://mls.jpl.nasa.gov, 2022.

Luo, B. P., Carslaw, K. S., Peter, T., and Clegg, S. L.: Vapour pressures of $H_2SO_4/HNO_3/HCl/HBr/H_2O$ solutions to low stratospheric temperatures, Geophys. Res. Lett., 22, 247–250, https://doi.org/10.1029/94GL02988, 1995.

Ma, C., Su, H., Lelieveld, J., Randel, W., Yu, P., Andreae, M. O., and Cheng, Y.: Smoke-charged vortex doubles hemispheric aerosol in the middle stratosphere and buffers ozone depletion, Sci. Adv., 10, eadn3657, https://doi.org/10.1126/sciadv.adn3657, 2024.

Metzger, S. and Lelieveld, J.: Reformulating atmospheric aerosol thermodynamics and hygroscopic growth into fog, haze and clouds, Atmos. Chem. Phys., 7, 3163–3193, https://doi.org/10.5194/acp-7-3163-2007, 2007.

Millán, L., Santee, M. L., Lambert, A., Livesey, N. J., Werner, F., Schwartz, M. J., Pumphrey, H. C., Manney, G. L., Wang, Y., Su, N., Wu, L., Read, W. G., and Froidevaux, L.: The Hunga Tonga-Hunga Ha'apai Hydration of the Stratosphere, Geophys. Res. Lett., 49, https://doi.org/10.1029/2022GL099381, 2022.

Ohneiser, K., Ansmann, A., Kaifler, B., Chudnovsky, A., Barja, B., Knopf, D. A., Kaifler, N., Baars, H., Seifert, P., Villanueva, D., Jimenez, C., Radenz, M., Engelmann, R., Veselovskii, I., and Zamorano, F.: Australian wildfire smoke in the stratosphere: the decay phase in 2020/2021 and impact on ozone depletion, Atmos. Chem. Phys., 22, 7417–7442, https://doi.org/10.5194/acp-22-7417-2022, 2022.

Osborne, M. J., de Leeuw, J., Witham, C., Schmidt, A., Beckett, F., Kristiansen, N., Buxmann, J., Saint, C., Welton, E. J., Fochesatto, J., Gomes, A. R., Bundke, U., Petzold, A., Marenco, F., and Haywood, J.: The 2019 Raikoke volcanic eruption – Part 2: Particle-phase dispersion and concurrent wildfire smoke emissions, Atmos. Chem. Phys., 22, 2975–2997, https://doi.org/10.5194/acp-22-2975-2022, 2022.

Peterson, D. A., Campbell, J. R., Hyer, E. J., Fromm, M. D., Kablick III, G. P., Cossuth, J. H., and DeLand, M. T.: Wildfire-driven thunderstorms cause a volcano-like stratospheric injection of smoke, npj Climate and Atmospheric Science, 30, 1, https://doi.org/10.1038/s41612-018-0039-3, 2018.

Peterson, D. A., Fromm, M. D., McRae, R. H. D., Campbell, J. R., Hyer, E. J., Taha, G., Camacho, C. P., Kablick III, G. P., Schmidt, C. C., and DeLand, M. T.: Australia's Black Summer pyrocumulonimbus super outbreak reveals potential for increasingly extreme stratospheric smoke events, npj Climate and Atmospheric Science, 38, 4, https://doi.org/0.1038/s41612-021-00192-9, 2021.

Pringle, K. J., Tost, H., Metzger, S., Steil, B., Giannadaki, D., Nenes, A., Fountoukis, C., Stier, P., Vignati, E., and Lelieveld, J.: Description and evaluation of GMXe: a new aerosol submodel for global simulations (v1), Geosci. Model Dev., 3, 391–412, https://doi.org/10.5194/gmd-3-391-2010, 2010.

Rieger, L. A., Zawada, D. J., Bourassa, A. E., and Degenstein, D. A.: A Multiwavelength Retrieval Approach for Improved OSIRIS Aerosol Extinction Retrievals, J. Geophys. Res.-Atmos., 124, 7286–7307, https://doi.org/10.1029/2018JD029897, 2019.

Rieger, L. A., Randel, W. J., Bourassa, A. E., and Solomon, S.: Stratospheric temperature and ozone anomalies associated with the 2020 Australian New Year fires, Geophys. Res. Lett., 48, https://doi.org/10.1029/2021GL095898, 2021.

Salawitch, R. J. and McBride, L. A.: Australian wildfires depleted the ozone layer, Science, 378, 830, https://doi.org/10.1126/science.add2056, 2022.

Santee, M. L., Lambert, A., Manney, G. L., Livesey, N. J., Froidevaux, L., Neu, J. L., Schwartz, M. J., Millán, L. F., Werner, F., Read, W. G., Park, M., Fuller, R. A., and Ward, B. M.: Prolonged and Pervasive Perturbations in the Composition of the Southern Hemisphere Midlatitude Lower Stratosphere From the Australian New Year's Fires, Geophys. Res. Lett., 49, https://doi.org/10.1029/2021GL096270, 2022.

Santee, M. L., Lambert, A., Froidevaux, L., Manney, G. L., Schwartz, M. J., Millán, L. F., Livesey, N. J., Read, W. G., Werner, F., and Fuller, R. A.: Strong evidence of heterogeneous processing on stratospheric sulfate aerosol in the extrapolar Southern Hemisphere following the 2022 Hunga Tonga-Hunga Ha'apai eruption, J. Geophys. Res. -Atmos., 128, https://doi.org/10.1029/2023JD039169, 2023.

Santee, M. L., Manney, G. L., Lambert, A., Millán, L. F., Livesey, N. J., Pitts, M. C., Froidevaux, L., Read, W. G., and Fuller, R. A.: The Influence of Stratospheric Hydration From the Hunga Eruption on Chemical Processing in the 2023 Antarctic Vortex, J. Geophys. Res. -Atmos., 129, https://doi.org/10.1029/2023JD040687, 2024.

Schallock, J., Brühl, C., Bingen, C., Höpfner, M., Rieger, L., and Lelieveld, J.: Reconstructing volcanic radiative forcing since 1990, using a comprehensive emission inventory and spatially resolved sulfur injections from satellite data in a chemistry-climate model, Atmos. Chem. Phys., 23, 1169–1207, https://doi.org/10.5194/acp-23-1169-2023, 2023.

Senf, F., Heinold, B., Kubin, A., Müller, J., Schrödner, R., and Tegen, I.: How the extreme 2019–2020 Australian wildfires affected global circulation and adjustments, Atmos. Chem. Phys., 23, 8939–8958, https://doi.org/10.5194/acp-23-8939-2023, 2023.

Solomon, S., Stone, K., Yu, P., Murphy, D. M., Kinnison, D., Ravishankara, A. R., and Wang, P.: Chlorine activation and enhanced ozone depletion induced by wildfire aerosol, Nature, 615, 259–264, https://doi.org/10.1038/s41586-022-05683-0, 2023.

Strahan, S. E., Smale, D., Solomon, S., Taha, G., Damon, M. R., Steenrod, S. D., Jones, N., Liley, B., Querel, R., and Robinson, J.: Unexpected repartitioning of stratospheric inorganic chlorine after the 2020 Australian wildfires, Geophys. Res. Lett., 49, https://doi.org/10.1029/2022GL098290, 2022.

Taha, G., Loughman, R., Colarco, P. R., Zhu, T., Thomason, L. W., and Jaross, G.: Tracking the 2022 Hunga Tonga-Hunga Ha'apai aerosol cloud in the upper and middle stratosphere using space-based observations, Geophys. Res. Lett., 49, https://doi.org/10.1029/2022GL100091, 2022.

Vescovini, T., P., N., Mallet, M., and Solmon, F.: Aerosol Direct Radiative Effects From Extreme Fire Events in Australia, California and Siberia Occurring in 2019–2020, J. Geophys. Res. -Atmos., 129, e2024JD041 002, https://doi.org/10.1029/2024JD041002, 2024.

Wang, X., Randel, W., Zhu, Y., Tilmes, S., Starr, J., Yu, W., Garcia, R., Toon, O., Park, M., Kinnison, D., Zhang, J., Bourassa, A., Rieger, L., Warnock, T., and Li, J.: Stratospheric climate anomalies and ozone loss caused by the Hunga Tonga-Hunga Ha'apai volcanic eruption, J. Geophys. Res. -Atmos., 128, https://doi.org/10.1029/2023JD039480, 2023.

Yu, P., Davis, S. M., Toon, O. B., Portmann, R. W., Bardeen, C. G., Barnes, J. E., Telg, H., and Maloney, C. Rosenlof, K. H.: Persistent stratospheric warming due to 2019–2020 Australian wildfire smoke, Geophys. Res. Lett., 48, e2021GL092 609, https://doi.org/10.1029/2021GL092609, 2021.

Zhang, J., Kinnison, D., Zhu, Y.and Wang, X., Tilmes, S., Dube, K., and Randel, W.: Chemistry Contribution to Stratospheric Ozone Depletion After the Unprecedented Water-Rich Hunga Tonga Eruption, Geophys. Res. Lett., 51, https://doi.org/10.1029/2023GL105762, 2024.

Zhu, Y., Bardeen, C. G., Tilmes, S., Mills, M. J., Wang, X., Harvey, V. L., Taha, G., Kinnison, D., Portmann, R. W., Yu, P., Rosenlof, K. H., Avery, M., Kloss, C., Li, C., Glanville, A. S., Millán, L., Deshler, T., Krotkov, N., and Toon, O. B.: Perturbations in stratospheric aerosol evolution due to the water-rich plume of the 2022 Hunga-Tonga eruption, Comm. Earth Env., https://doi.org/10.1038/s43247-022-00580-w, 2022.

Zhu, Y., Portmann, R. W., Kinnison, D., Toon, O. B., Millán, L., Zhang, J., Vömel, H., Tilmes, S., Bardeen, C. G., Wang, X., Evan, S., Randel, W. J., and Rosenlof, K. H.: Stratospheric ozone depletion inside the volcanic plume shortly after the 2022 Hunga Tonga eruption, Atmos. Chem. Phys., 23, 13 355–13 367, https://doi.org/10.5194/acp-23-13355-2023, 2023.

Appendix A: Additional figures

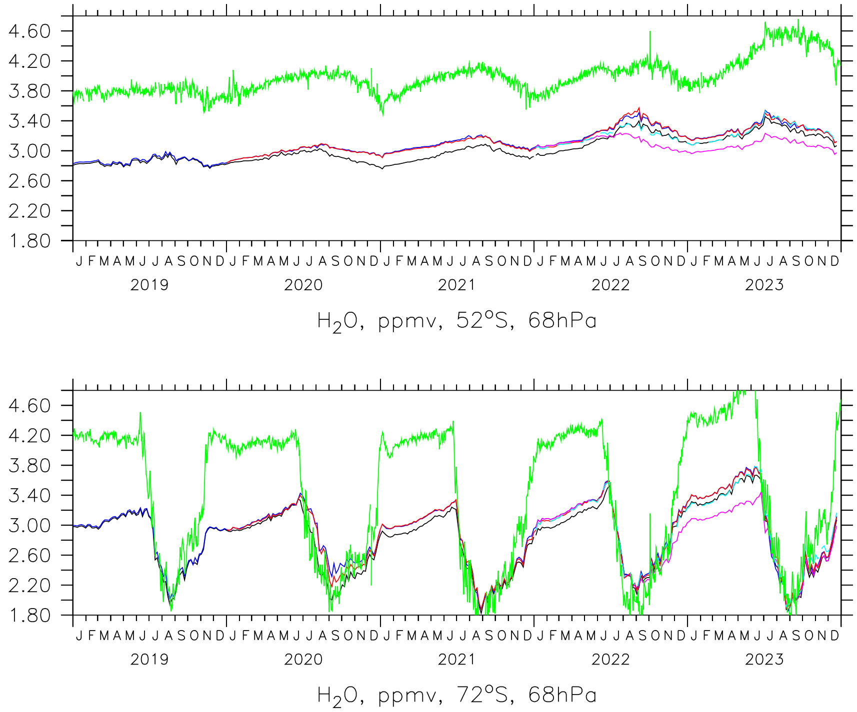

Figure A1. Calculated and observed water vapor, colors as in Fig. 7. Lightblue dashed is the sensitivity study with co-injected SO_2 and H_2O.

This section provides the comparison of water vapour simulated by EMAC with MLS observations (Fig. A1) and simulated NO_2 (Fig. A2) and HO_2 (Fig. A3) as rate limiting radicals for catalytic ozone destruction. Further number density (Fig. A4) and median radius (Fig. A5, for effective radius multiply by 1.49) for the accumulation mode of stratospheric aerosol are shown, as well as total radiative (solar+thermal) aerosol heating rates (Figs. A6 and A7) and examples for self lofting smoke filled vortices and the corresponding ozone reduction calculated by EMAC (Figs. A8 and A9).

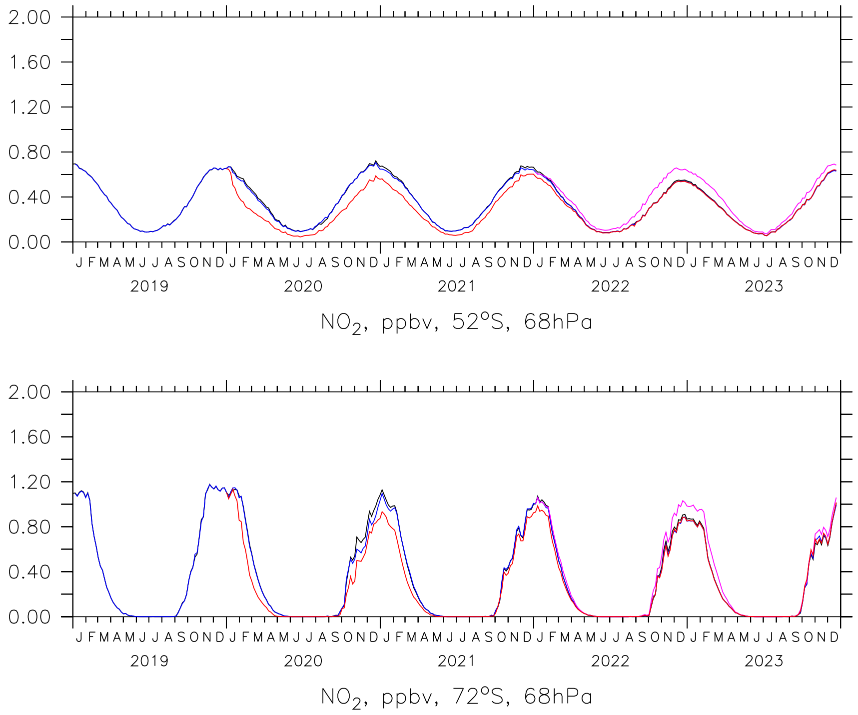

NO_2, ppbv, 52°S, 68hPa

NO_2, ppbv, 72°S, 68hPa

Figure A2. Calculated NO_2, colors as in Fig. 3.

https://doi.org/10.5194/egusphere-2025-2981
Preprint. Discussion started: 27 June 2025

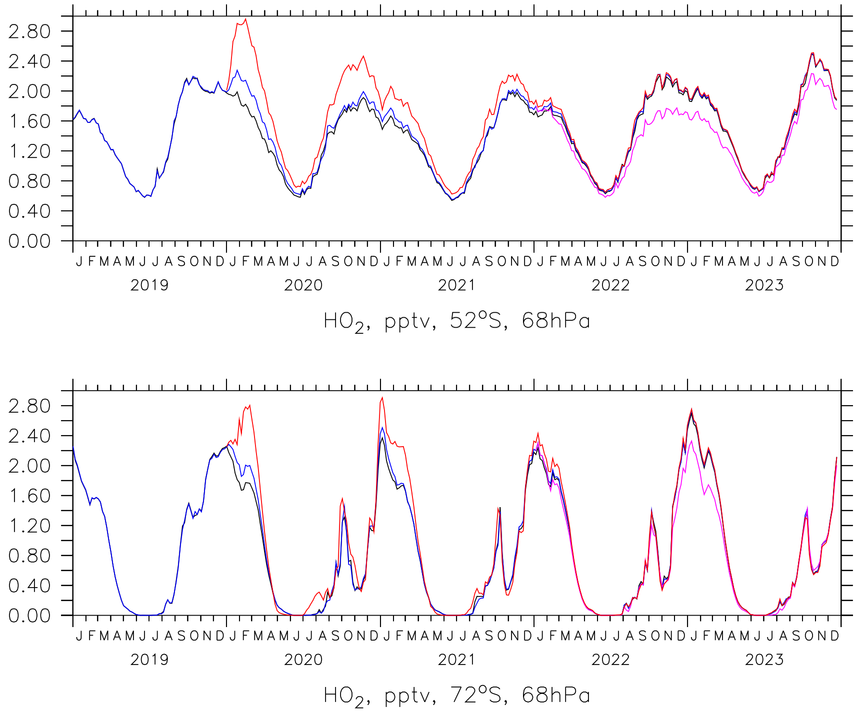

Figure A3. Calculated HO_2, colors as in Fig. 3.

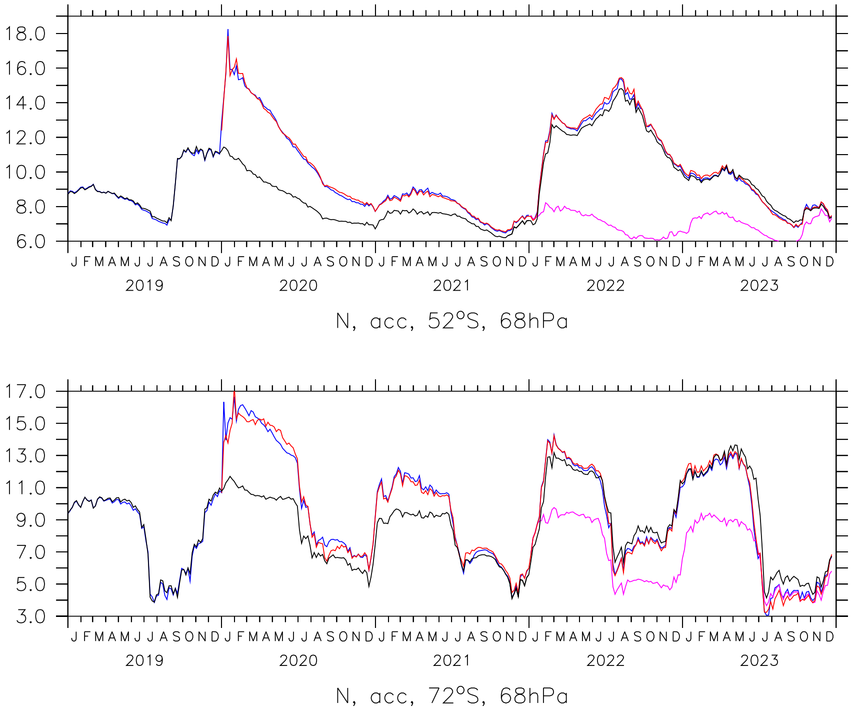

N, acc, 52°S, 68hPa

N, acc, 72°S, 68hPa

Figure A4. Calculated particle number density (accumulation mode, 1/cm^3), colors as in Fig. 3.

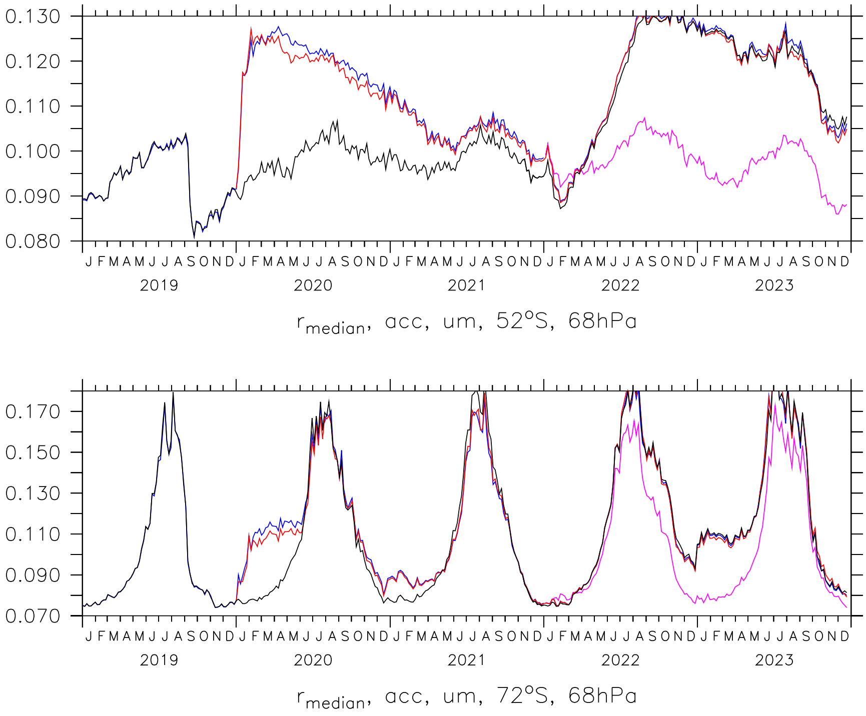

Figure A5. Calculated median particle radius (accumulation mode, μm), colors as in Fig. 3.

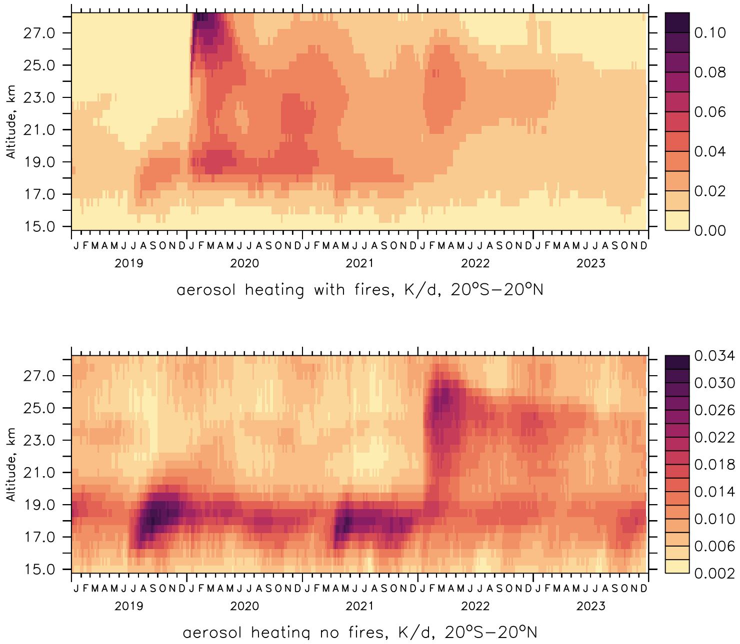

Figure A6. Calculated aerosol radiative heating rates in tropics.

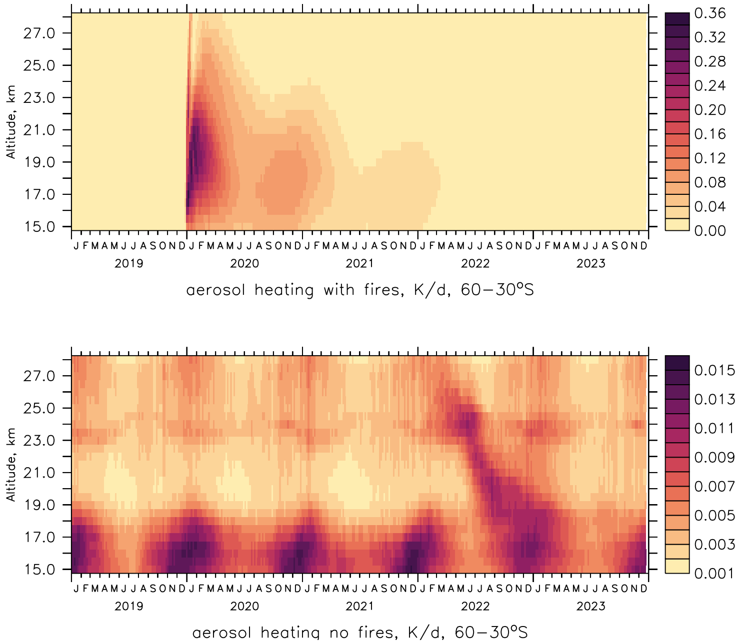

Figure A7. Calculated aerosol radiative heating rates in SH midlatitudes.

https://doi.org/10.5194/egusphere-2025-2981
Preprint. Discussion started: 27 June 2025

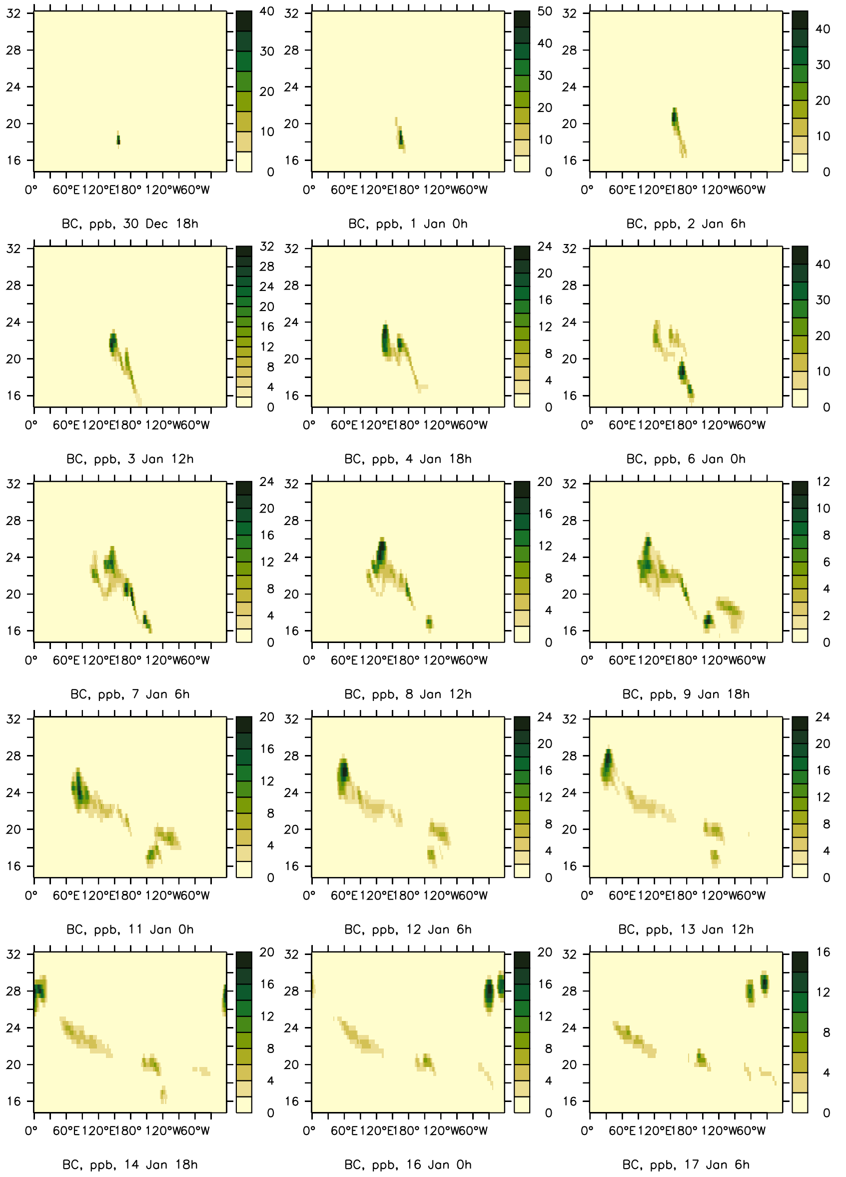

BC, ppb, 30 Dec 18h

BC, ppb, 1 Jan 0h

BC, ppb, 2 Jan 6h

BC, ppb, 3 Jan 12h

BC, ppb, 4 Jan 18h

BC, ppb, 6 Jan 0h

BC, ppb, 7 Jan 6h

BC, ppb, 8 Jan 12h

BC, ppb, 9 Jan 18h

BC, ppb, 11 Jan 0h

BC, ppb, 12 Jan 6h

BC, ppb, 13 Jan 12h

BC, ppb, 14 Jan 18h

BC, ppb, 16 Jan 0h

BC, ppb, 17 Jan 6h

Figure A8. Simulated BC in lofting vortices every 30h at 35^{o}S against altitude in km.

https://doi.org/10.5194/egusphere-2025-2981
Preprint. Discussion started: 27 June 2025

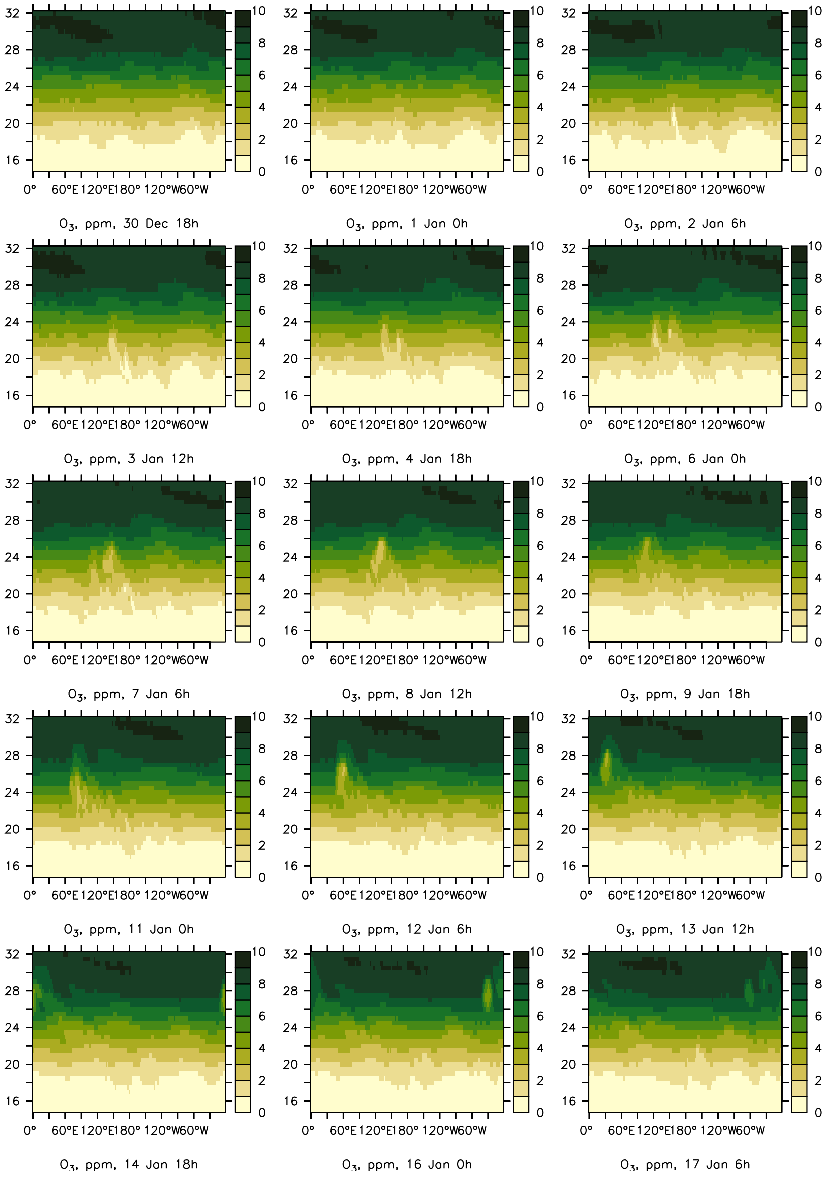

O_3, ppm, 30 Dec 18h

O_3, ppm, 1 Jan 0h

O_3, ppm, 2 Jan 6h

O_3, ppm, 3 Jan 12h

O_3, ppm, 4 Jan 18h

O_3, ppm, 6 Jan 0h

O_3, ppm, 7 Jan 6h

O_3, ppm, 8 Jan 12h

O_3, ppm, 9 Jan 18h

O_3, ppm, 11 Jan 0h

O_3, ppm, 12 Jan 6h

O_3, ppm, 13 Jan 12h

O_3, ppm, 14 Jan 18h

O_3, ppm, 16 Jan 0h

O_3, ppm, 17 Jan 6h

Figure A9. Simulated depleted ozone in the vortices of Fig. A8.